LETTER

doi:10.1038/nature10230

A forty-kilodalton protein of the inner membrane is the mitochondrial calcium uniporter

Diego De Stefani[1,2]*, Anna Raffaello[1,2]*, Enrico Teardo[3], Ildikò Szabò[3] & Rosario Rizzuto[1,2]

Mitochondrial Ca^{2+} homeostasis has a key role in the regulation of aerobic metabolism and cell survival[1], but the molecular identity of the Ca^{2+} channel, the mitochondrial calcium uniporter[2], is still unknown. Here we have identified *in silico* a protein (named MCU) that shares tissue distribution with MICU1 (also known as CBARA1), a recently characterized uniporter regulator[3], is present in organisms in which mitochondrial Ca^{2+} uptake was demonstrated and whose sequence includes two transmembrane domains. Short interfering RNA (siRNA) silencing of MCU in HeLa cells markedly reduced mitochondrial Ca^{2+} uptake. MCU overexpression doubled the matrix Ca^{2+} concentration increase evoked by inositol 1,4,5-trisphosphate-generating agonists, thus significantly buffering the cytosolic elevation. The purified MCU protein showed channel activity in planar lipid bilayers, with electrophysiological properties and inhibitor sensitivity of the uniporter. A mutant MCU, in which two negatively charged residues of the putative pore-forming region were replaced, had no channel activity and reduced agonist-dependent matrix Ca^{2+} concentration transients when overexpressed in HeLa cells. Overall, these data demonstrate that the 40-kDa protein identified is the channel responsible for ruthenium-red-sensitive mitochondrial Ca^{2+} uptake, thus providing a molecular basis for this process of utmost physiological and pathological relevance.

The past two decades have seen the re-appraisal of the key role of mitochondria in decoding the highly pleiotropic Ca^{2+} signals evoked by physiological and pathological stimuli[4]. Mitochondria undergo rapid changes in matrix Ca^{2+} concentration ($[Ca^{2+}]_{mt}$) upon cell stimulation, because their low affinity uptake systems are exposed to microdomains of high $[Ca^{2+}]$ in proximity to endoplasmic reticulum or plasma membrane Ca^{2+} channels[5–9]. In turn, $[Ca^{2+}]_{mt}$ increases upregulate aerobic metabolism[10,11] and sensitize mitochondria to apoptotic challenges, favouring the release of caspase cofactors[12,13]. Mitochondrial Ca^{2+} buffering also shapes the amplitude and spatio-temporal patterns of cytosolic Ca^{2+} concentration ($[Ca^{2+}]_{cyt}$) increases[14–16]. The properties of the Ca^{2+} transporter are still largely those characterized in the 1960s: (1) electrogenic transport (hence the name calcium 'uniporter'), then shown to be a highly selective channel[17], (2) sensitivity to ruthenium red, and (3) low affinity for the cation[1,2,18]. Its molecular identity, however, has remained elusive.

Recently, a uniporter regulator (named MICU1), necessary for rapid mitochondrial Ca^{2+} uptake in intact cells, was identified *in silico* in the MitoCarta database[3]. We thus looked in the same database for the actual transporter, that is, an integral inner membrane protein fulfilling the criteria for being the bona fide MCU. Among 529 candidates with ubiquitous expression in mammalian tissues, we restricted the analysis to 89 proteins with two or more predicted transmembrane domains in the primary sequence. Of these, 20 were absent in *Saccharomyces cerevisiae* (lacking a RuR-sensitive mitochondrial Ca^{2+} uptake route[19]), and, among those, 14 were significantly conserved also in kinetoplastids (*Trypanosoma* and *Leishmania*), in which rapid, uncoupler-sensitive Ca^{2+} fluxes to mitochondria were measured[20,21]. This list (Supplementary Table 1) included 13 proteins with either already characterized functions (complex I subunits, assembly regulators, and so on) or poor alignment scores. The remaining protein (NP_001028431) includes a highly conserved domain comprising two transmembrane regions and an intervening loop enriched in acidic residues (Fig. 1a), indicative of a possible common role in cation permeation. This domain was also detected by hidden Markov model-based analysis of evolutionary conserved proteins (Pfam PF04678 and Panther PTHR1346 domains, with undefined function), further supporting the significance of the hit. We thus considered this protein a putative mitochondrial Ca^{2+} channel, named it MCU (mitochondrial calcium uniporter) and characterized it in detail. Tissue expression profiling by real-time PCR showed ubiquitous presence in all investigated tissues (Fig. 1b), in agreement with a housekeeping role, with expression levels correlating with those of MICU1.

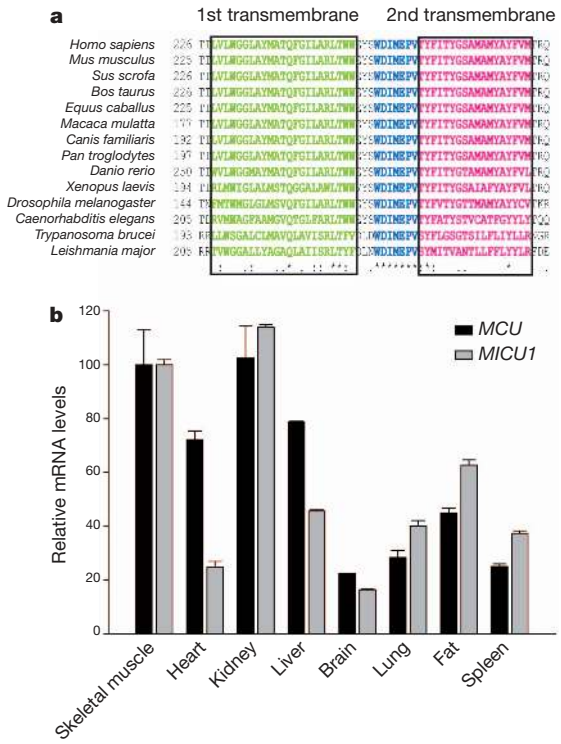

Figure 1 | MCU includes two highly conserved transmembrane domains and is ubiquitously expressed in mammals, similarly to its putative regulator MICU1. a, Alignment of the putative transmembrane domain and pore region of MCU proteins from 14 different species . **b**, Real-time PCR analysis of mouse tissues. mRNA extraction and real-time PCR was as described in the Methods section. Expression levels are normalized to skeletal muscle, and presented as means ± s.d. ($n = 3$).

[1]Departments of Biomedical Sciences, University of Padua, 35121 Padua, Italy. [2]CNR Institute of Neuroscience, University of Padua, 35121 Padua, Italy. [3]Department of Biology, University of Padua, 35121 Padua, Italy.
*These authors contributed equally to this work

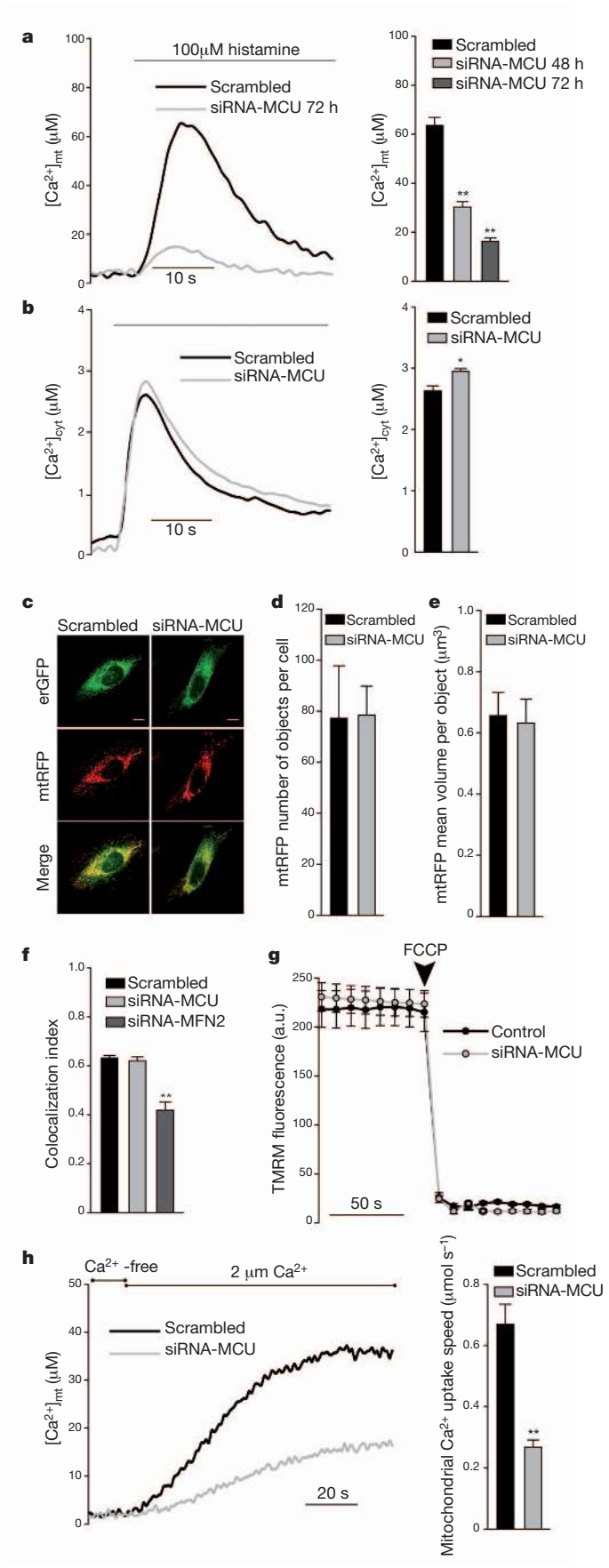

To verify the role of MCU in mitochondrial Ca^{2+} handling, siRNA oligonucleotides were synthesized and tested (Supplementary Fig. 1), Ca^{2+} measurements were then carried out with aequorin-based mitochondrial and cytosolic Ca^{2+} probes (mtAEQ and cytAEQ) (Fig. 2a and Supplementary Fig. 1). MCU-silenced and control HeLa cells, perfused with modified Krebs–Ringer buffer supplemented with 1 mM $CaCl_2$ (KRB), were challenged, where indicated, with 100 μM histamine, an inositol 1,4,5-trisphosphate-generating agonist causing Ca^{2+} release from the endoplasmic reticulum. In control cells, the $[Ca^{2+}]_{mt}$ rise evoked by histamine stimulation was ~63 μM (Fig. 2a). In MCU-silenced cells mitochondrial Ca^{2+} accumulation was markedly reduced (peak value ~30 μM and ~16 μM 48 h and 72 h after silencing, respectively). The marked reduction was specific of mitochondria, as $[Ca^{2+}]_{cyt}$ rises were almost unaffected (rather, a small but significant increase was detected, possibly due to reduced mitochondrial buffering) (Fig. 2b). Overexpression of MICU1 did not rescue the $[Ca^{2+}]_{mt}$ reduction in MCU-silenced cells, and had a marginal effect in control cells (Supplementary Fig. 2). Experiments were then carried out to exclude that the observed effect was secondary to changes in mitochondrial morphology (that is, fragmentation, swelling or redistribution away from the endoplasmic reticulum) or in the driving force for Ca^{2+} accumulation (that is, a collapse of mitochondrial membrane potential, $\Delta\Psi$). On the former aspect, mitochondria and endoplasmic reticulum were labelled in living cells by co-expressing red and green fluorescent protein specifically targeted to the mitochondria and endoplasmic reticulum compartments (mtRFP and erGFP; Fig. 2c and Supplementary Fig. 3). mtRFP imaging showed the typical three-dimensional interconnected network, with no difference in mitochondrial number and volume between control and MCU-silenced cells (Fig. 2d, e). Also the endoplasmic reticulum showed a similar distribution in control and MCU-silenced cells, and no difference was detected in the number of mtRFP/erGFP fluorescence overlaps, whereas in cells in which the endoplasmic reticulum/mitochondria tether mitofusin 2 (*MFN2*)[22] was silenced a marked reduction was observed (Fig. 2f and Supplementary Fig. 3). As to the driving force for Ca^{2+} uptake, no difference was detected in the loading of the fluorescent dye tetramethyl rhodamine methyl ester (TMRM) (Fig. 2g), thus ruling out a $\Delta\Psi$ drop in MCU-silenced cells. In brief, mitochondria simply seem to have an intrinsically reduced ability of accumulating Ca^{2+}. Direct evidence was obtained by permeabilizing MCU-silenced and control cells in intracellular buffer, containing 100 μM EGTA (Ca^{2+}-free) and then imposing an EGTA-buffered fixed $[Ca^{2+}]$ of 2 μM (2 μM Ca^{2+}). Under those conditions, in MCU-silenced cells Ca^{2+} uptake was initiated at a speed that was threefold lower than controls (Fig. 2h).

To demonstrate that MCU promotes Ca^{2+} uptake, overexpression experiments were carried out. The full-length complementary DNA of the protein, obtained by PCR after reverse transcription from skeletal muscle RNA, was identical to that deposited in the NCBI databank (NM_001033259). The cDNA was cloned in pcDNA3.1 and co-expressed with aequorin probes. MCU-overexpressing cells showed a marked increase in the histamine-evoked $[Ca^{2+}]_{mt}$ rise (106%, ~169 μM in MCU-overexpressing vs ~82 μM in control cells, Fig. 3a). The greater mitochondrial response was not secondary to

Figure 2 | MCU silencing strongly inhibits mitochondrial Ca^{2+} uptake without causing morphological rearrangement or changes in the electrochemical gradient. **a**, **b**, Measurement of $[Ca^{2+}]_{mt}$ (**a**) and $[Ca^{2+}]_{cyt}$ (**b**) in MCU-silenced cells. **c**, Fluorescence images of mtRFP- and erGFP-labelled mitochondria and endoplasmic reticulum, respectively. **d**, **e**, Mitochondrial number and volume, as deduced by calculating object number (**d**) and size (**e**). **f**, endoplasmic reticulum/mitochondria colocalization, estimated by Pearson's correlation coefficient. **g**, TMRM fluorescence measurements. a.u., arbitrary units. **h**, $[Ca^{2+}]_{mt}$ measurements in permeabilized cells. In this and following figures, experiments are representative of more than five trials, conditions are in the Methods section, and statistics in Supplementary Table 2. $^{*}P < 0.05$, $^{**}P < 0.001$. Error bars correspond to mean ± s.e.m.

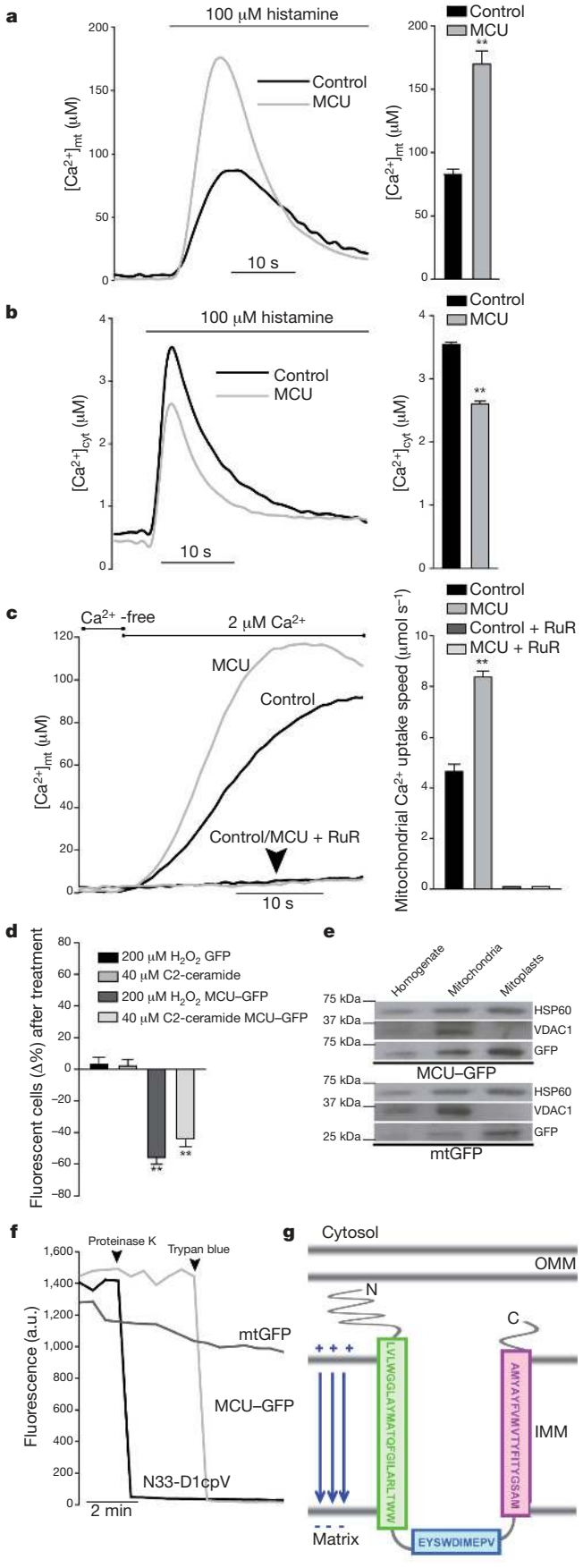

alterations of the cytosolic response. Rather, a significant reduction in the $[Ca^{2+}]_{cyt}$ transient was observed, most probably because of increased Ca^{2+} clearance by mitochondria (Fig. 3b). Enhanced mitochondrial Ca^{2+} uptake was confirmed also upon capacitative Ca^{2+} influx (Supplementary Fig. 4) and in permeabilized cells (Fig. 3c). As in Fig. 2h, mitochondrial Ca^{2+} uptake was initiated by switching the medium, after digitonin permeabilization, from intracellular buffer/EGTA (Ca^{2+}-free) to intracellular buffer/Ca^{2+} (3 μM Ca^{2+}). MCU-overexpressing cells showed a faster rate of Ca^{2+} uptake and reached a higher plateau level (Fig. 3c). Finally, we verified whether the increased intrinsic ability of mitochondria to accumulate Ca^{2+} correlated with sensitivity to apoptotic challenges (Fig. 3d). Microscopy counts of cell viability after treatment with C2-ceramide or H_2O_2 showed that MCU-expressing cells were more efficiently killed, thus confirming the notion that mitochondrial Ca^{2+} loading synergizes with these apoptotic stimuli[12,23].

We then investigated the subcellular distribution of MCU. For this purpose, tagged versions of MCU were generated (MCU–GFP and MCU–Flag), that had the same effect on $[Ca^{2+}]_{mt}$ as MCU (Supplementary Fig. 5). GFP fluorescence and immunocytochemistry labelling with anti-Flag antibody completely overlapped with mitochondrial markers (Supplementary Fig. 6). Then, intra-mitochondrial distribution and topology was investigated. HeLa cells were transfected with MCU–GFP (or the matrix probe mtGFP) and harvested. The mitochondrial fraction was obtained by differential centrifugation and either blotted directly, or subjected to osmotic swelling, thus obtaining the mitoplast fraction devoid of the outer membrane. Both MCU and mtGFP were progressively more enriched in the mitochondrial and mitoplast fractions (Fig. 3e). Mitochondrial localization was also confirmed by immuno-electron microscopy of HeLa cells expressing MCU–Flag (Supplementary Fig. 7). To show the inner membrane localization and get information on the topology of MCU, we carried out an experiment in digitonin-permeabilized cells, in which GFP fluorescence was visualized before and after treatment with proteinase K or Trypan blue, a fluorescence quencher that crosses the outer, but not the inner mitochondrial membrane[9] (Fig. 3f). Proteinase K had no effect on MCU–GFP fluorescence (but abrogated fluorescence of the cytosolic, outer mitochondrial membrane-anchored N33-D1cpV probe, confirming that MCU is not on the outer mitochondrial membrane), whereas Trypan blue abrogated MCU–GFP (but not mtGFP) fluorescence (Fig. 3f), thus demonstrating that MCU is in the inner mitochondrial membrane, with the carboxy terminus most probably located in the intermembrane space (Fig. 3g).

Finally, we investigated the channel activity of the purified protein reconstituted in a planar lipid bilayer. For this purpose, a His-tagged MCU was generated and expressed in two different heterologous expression systems, *Escherichia coli* and wheat-germ cell-free transcription/translation. The purified protein (Supplementary Fig. 8) was inserted into lipid bilayers, and its electrophysiological activity was assessed in a medium containing only Ca^{2+} as cation. With both preparations, we measured channel activity, with the properties previously reported for the uniporter[17,24]: conductance of 6–7 pS (in the

Figure 3 | MCU overexpression increases mitochondrial Ca^{2+} accumulation in intact and permeabilized cells, buffers cytosolic $[Ca^{2+}]$ rises, and sensitizes to apoptotic stimuli; GFP-tagged MCU demonstrates mitochondrial localization and indicates a putative membrane topology. **a**, **b**, Measurement of $[Ca^{2+}]_{mt}$ (**a**) and $[Ca^{2+}]_{cyt}$ (**b**) in MCU-silenced cells. **c**, $[Ca^{2+}]_{mt}$ measurements in permeabilized cells. RuR, ruthenium red. **d**, Cell viability upon apoptotic challenge. **e**, Subcellular fractionation of MCU–GFP- and mtGFP-expressing cells and western blotting for GFP, matrix (HSP60) and outer mitochondrial membrane (VDAC1) markers. **f**, GFP proteinase K degradation and fluorescence quenching by Trypan blue in permeabilized cells transfected with mtGFP, MCU–GFP or N33-D1cpV. **g**, Schematic representation of the predicted MCU topology. IMM, inner mitochondrial membrane; OMM, outer mitochondrial membrane. $^{**}P < 0.001$. Error bars: **a**–**c**, mean ± s.e.m.; **d**, **f**, mean ± s.d.

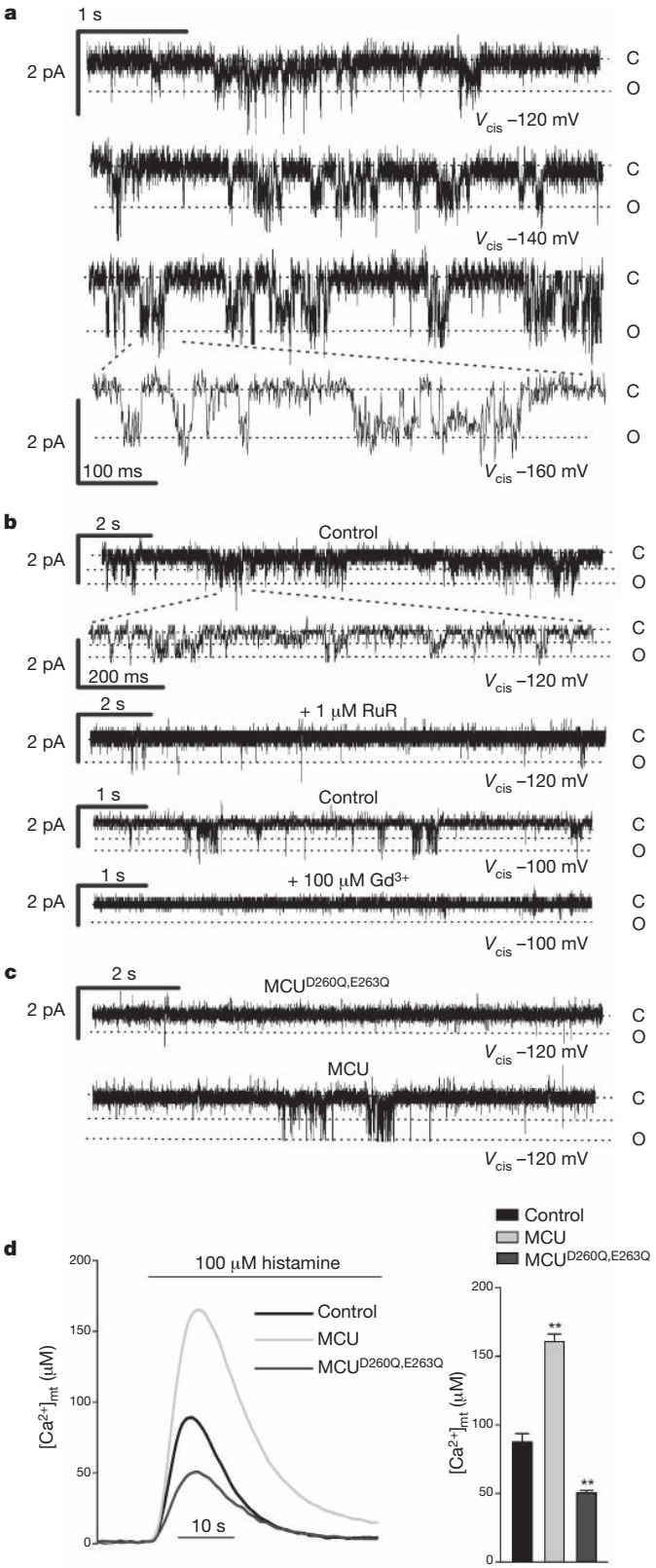

Figure 4 | Purified MCU shows channel activity in lipid bilayers, whereas $MCU^{D260Q,E263Q}$ shows no channel activity and reduces $[Ca^{2+}]_{mt}$ transients in cells. **a**–**c**, Electrophysiological recordings of purified MCU or $MCU^{D260Q,E263Q}$, produced in *E. coli* (**a** and **b**) or *in vitro* (**c**) and reconstituted in planar lipid bilayers. C, closed; O, opened; V_{cis}, voltage applied to the *cis* side. **a**, MCU traces at different applied voltages; **b**, MCU traces before and after addition of RuR or Gd^{3+}; **c**, $MCU^{D260Q,E263Q}$ traces. After 10 min recording with no current, MCU was added and channel activity was detected after 1–2 min (lower trace). **d**, $[Ca^{2+}]_{mt}$ measurements in $MCU^{D260Q,E263Q}$-expressing cells. Error bars correspond to mean ± s.e.m.

negative voltage range applied in the *cis* compartment), fast kinetics, low probability of opening at low voltages (P_o), P_o increase with voltage, and inhibition by ruthenium red and the lanthanide gadolinium (Gd^{3+}) (Fig. 4a and b and Supplementary Fig. 9). Then, to get evidence of cation permeation across the putative pore-forming domain, we mutated into glutamines two negatively charged residues of the conserved region (D260Q and E263Q) and assessed the electrophysiological properties of the mutant protein ($MCU^{D260Q,E263Q}$) produced *in vitro*. $MCU^{D260Q,E263Q}$ failed to give rise to Ca^{2+}-permeable channel activity in bilayer experiments, whereas in the same membrane the subsequent addition of MCU initiated channel activity with the characteristics described above (Fig. 4c). $MCU^{D260Q,E263Q}$, when overexpressed in HeLa cells, showed the same membrane topology as MCU (Supplementary Fig. 10) and caused a marked reduction in histamine-induced $[Ca^{2+}]_{mt}$ rises, both compared to MCU-overexpressing and control cells (Fig. 4d). $MCU^{D260Q,E263Q}$ thus acts as a dominant-negative mutant, most probably by either inhibiting MCU channel activity within an oligomer or competing for docking sites or essential regulators.

In conclusion, we have identified a 40-kDa protein which fulfils the requirements for being the long searched for mitochondrial calcium uniporter: it contains two transmembrane domains and shows channel activity *in vitro* with the previously characterized properties of the uniporter, it is localized in the inner membrane and, finally, it markedly enhances mitochondrial Ca^{2+} uptake upon overexpression. The availability of molecular information opens the mitochondrial checkpoint in cellular Ca^{2+} signalling to a deeper understanding. Informative animal models can now be generated and new drugs developed to influence processes regulated by mitochondrial Ca^{2+} signals, such as aerobic metabolism and cell death.

METHODS SUMMARY

Candidate mouse genes coding for the mitochondrial calcium uniporter were searched starting from the MitoCarta database. Bioinformatic analysis was performed by selecting candidates according to the following parameters: (1) genes expressed in most mammalian tissues, (2) the presence of two or more transmembrane domains, (3) without any homologues in *Saccharomyces cerevisiae* but (4) conserved in kinetoplastids. The resulting 14 candidates were manually screened to search for highly conserved putative channel-forming domains.

All the experiments were performed in HeLa cells. MCU was silenced using specific siRNAs. The MCU cDNA was retro-transcribed and amplified from mouse skeletal muscle messenger RNA and overexpressed after cloning in several expression plasmids.

$[Ca^{2+}]_{cyt}$ and $[Ca^{2+}]_{mt}$ were measured in MCU-silenced and MCU-overexpressing cells using appropriate cytosolic and mitochondrial probes[25].

Morphology of MCU-silenced cells was evaluated using GFP and RFP specifically targeted to the mitochondria and endoplasmic reticulum compartments (erGFP and mtRFP)[6].

MCU mitochondrial localization was demonstrated by confocal imaging of cells transfected with the MCU–GFP expression vector and loaded with MitoTracker Red and by fractionation and western blotting of cells overexpressing MCU–GFP, as previously described[26].

Reconstitution in planar lipid bilayer was carried out with the purified protein from both *E. coli* and *in vitro* transcription/translation using 100 mM $CaCl_2$. Bilayers of approximately 150–200 pF capacity were prepared using purified soybean azolectin.

Full Methods and any associated references are available in the online version of the paper at www.nature.com/nature.

Received 29 December 2010; accepted 27 May 2011.
Published online 19 June 2011.

1. Szabadkai, G. & Duchen, M. R. Mitochondria: the hub of cellular Ca^{2+} signaling. *Physiology (Bethesda)* **23,** 84–94 (2008).
2. Carafoli, E. Historical review: mitochondria and calcium: ups and downs of an unusual relationship. *Trends Biochem. Sci.* **28,** 175–181 (2003).

3. Perocchi, F. *et al. MICU1* encodes a mitochondrial EF hand protein required for Ca^{2+} uptake. *Nature* **467,** 291–296 (2010).
4. Berridge, M. J., Bootman, M. D. & Roderick, H. L. Calcium signalling: dynamics, homeostasis and remodelling. *Nature Rev. Mol. Cell Biol.* **4,** 517–529 (2003).
5. Rizzuto, R., Brini, M., Murgia, M. & Pozzan, T. Microdomains with high Ca^{2+} close to IP3-sensitive channels that are sensed by neighboring mitochondria. *Science* **262,** 744–747 (1993).
6. Rizzuto, R. *et al.* Close contacts with the endoplasmic reticulum as determinants of mitochondrial Ca^{2+} responses. *Science* **280,** 1763–1766 (1998).
7. Csordás, G., Thomas, A. P. & Hajnóczky, G. Quasi-synaptic calcium signal transmission between endoplasmic reticulum and mitochondria. *EMBO J.* **18,** 96–108 (1999).
8. Csordás, G. *et al.* Imaging interorganelle contacts and local calcium dynamics at the ER-mitochondrial interface. *Mol. Cell* **39,** 121–132 (2010).
9. Giacomello, M. *et al.* Ca^{2+} hot spots on the mitochondrial surface are generated by Ca^{2+} mobilization from stores, but not by activation of store-operated Ca^{2+} channels. *Mol. Cell* **38,** 280–290 (2010).
10. Hajnóczky, G., Robb-Gaspers, L. D., Seitz, M. B. & Thomas, A. P. Decoding of cytosolic calcium oscillations in the mitochondria. *Cell* **82,** 415–424 (1995).
11. Jouaville, L. S., Pinton, P., Bastianutto, C., Rutter, G. A. & Rizzuto, R. Regulation of mitochondrial ATP synthesis by calcium: evidence for a long-term metabolic priming. *Proc. Natl Acad. Sci. USA* **96,** 13807–13812 (1999).
12. Pinton, P. *et al.* The Ca^{2+} concentration of the endoplasmic reticulum is a key determinant of ceramide-induced apoptosis: significance for the molecular mechanism of Bcl-2 action. *EMBO J.* **20,** 2690–2701 (2001).
13. Pacher, P. & Hajnóczky, G. Propagation of the apoptotic signal by mitochondrial waves. *EMBO J.* **20,** 4107–4121 (2001).
14. Hajnóczky, G., Hager, R. & Thomas, A. P. Mitochondria suppress local feedback activation of inositol 1,4,5-trisphosphate receptors by Ca^{2+}. *J. Biol. Chem.* **274,** 14157–14162 (1999).
15. Boitier, E., Rea, R. & Duchen, M. R. Mitochondria exert a negative feedback on the propagation of intracellular Ca^{2+} waves in rat cortical astrocytes. *J. Cell Biol.* **145,** 795–808 (1999).
16. Tinel, H. *et al.* Active mitochondria surrounding the pancreatic acinar granule region prevent spreading of inositol trisphosphate-evoked local cytosolic Ca^{2+} signals. *EMBO J.* **18,** 4999–5008 (1999).
17. Kirichok, Y., Krapivinsky, G. & Clapham, D. E. The mitochondrial calcium uniporter is a highly selective ion channel. *Nature* **427,** 360–364 (2004).
18. Nicholls, D. G. Mitochondria and calcium signaling. *Cell Calcium* **38,** 311–317 (2005).
19. Uribe, S., Rangel, P. & Pardo, J. P. Interactions of calcium with yeast mitochondria. *Cell Calcium* **13,** 211–217 (1992).
20. Xiong, Z. H., Ridgley, E. L., Enis, D., Olness, F. & Ruben, L. Selective transfer of calcium from an acidic compartment to the mitochondrion of *Trypanosoma brucei*. Measurements with targeted aequorins. *J. Biol. Chem.* **272,** 31022–31028 (1997).
21. Benaim, G., Bermudez, R. & Urbina, J. A. Ca^{2+} transport in isolated mitochondrial vesicles from *Leishmania braziliensis* promastigotes. *Mol. Biochem. Parasitol.* **39,** 61–68 (1990).
22. de Brito, O. M. & Scorrano, L. Mitofusin 2 tethers endoplasmic reticulum to mitochondria. *Nature* **456,** 605–610 (2008).
23. Hajnóczky, G., Csordás, G., Madesh, M. & Pacher, P. Control of apoptosis by IP_3 and ryanodine receptor driven calcium signals. *Cell Calcium* **28,** 349–363 (2000).
24. Michels, G. *et al.* Regulation of the human cardiac mitochondrial Ca^{2+} uptake by 2 different voltage-gated Ca^{2+} channels. *Circulation* **119,** 2435–2443 (2009).
25. Pinton, P., Rimessi, A., Romagnoli, A., Prandini, A. & Rizzuto, R. Biosensors for the detection of calcium and pH. *Methods Cell Biol.* **80,** 297–325 (2007).
26. Wieckowski, M. R., Giorgi, C., Lebiedzinska, M., Duszynski, J. & Pinton, P. Isolation of mitochondria-associated membranes and mitochondria from animal tissues and cells. *Nature Protocols* **4,** 1582–1590 (2009).

Supplementary Information is linked to the online version of the paper at www.nature.com/nature.

Acknowledgements We thank M. Zoratti for help in the analysis of electrophysiological data, G. Merli for carrying out some of the experiments and P. Bernardi, T. Pozzan and L. Cendron for helpful discussions and for the N33-D1cpV expression plasmid (T. Pozzan). This research was supported by grants from the Italian Ministry of Education, University and Research, European Commission (FP7 ''MyoAGE'', no. 223576), National Institutes of Health (Grant #1P01AG025532-01A1), Cariparo Foundation (Padua), the Italian Association for Cancer Research (AIRC) and Telethon-Italy (GPP1005).

Author Contributions D.D.S. performed bioinformatic analysis, Ca^{2+} measurements and morphological analysis of organelles. A.R. performed molecular biology and gene expression analysis. D.D.S. and A.R. contributed equally to the study. E.T. expressed and purified the protein in heterologous systems; I.S. performed and analysed the electrophysiology experiments; R.R. discussed the results and wrote the paper.

Author Information Reprints and permissions information is available at www.nature.com/reprints. The authors declare no competing financial interests. Readers are welcome to comment on the online version of this article at www.nature.com/nature. Correspondence and requests for materials should be addressed to R.R. (rosario.rizzuto@unipd.it).

METHODS

Bioinformatic screening. The MitoCarta database was screened for ubiquitously expressed proteins (expressed in at least 12 out of 14 tissues analysed, obtaining 529 candidates) and proteins containing two or more transmembrane domains were selected using the TMHMM algorithm[27]. Out of 1,098 proteins present in MitoCarta, 89 fulfilled these requirements. Sequences of these candidates were retrieved and aligned with the *Saccharomyces cerevisiae* proteome by a standard Gonnet matrix to exclude homologues. All alignments with a P-value < 0.001 were excluded. Out of 89, 20 remained and were subsequently aligned with kinetoplastids proteomes using the TriTrypDB server. Out of 20, 14 had significant scores. These candidates were manually aligned through different species to look for putative highly conserved channel-forming domains.

RNA extraction and gene expression analyses. For the expression analysis of MCU and MICU1 in mouse tissues, adult male C57BL/6 mice (28–30 g) were used. Skeletal muscles (tibialis anterior), heart, brain, spleen, lung, liver, kidney and visceral fat were excised from three age-matched animals. Total RNA was purified using an SV Total RNA Isolation kit (Promega) following manufacturer instructions. The RNA was quantified and controlled for its quality using a RNA 6000 LabChip kit (Agilent Technologies) in conjunction with an Agilent Bioanalyzer 2001. An equal amount of total RNA from the three animals was pooled together for each organ, complementary DNA was generated with a cDNA synthesis kit (SuperScript VILO, Invitrogen) and analysed by real-time PCR using the SYBR green chemistry (Bio-Rad). The primers were designed and analysed with Primer3. Identity of the amplicons was confirmed by their dissociation profiles and gel analysis. Real-time PCR standard curves were constructed by using serial dilutions of pooled cDNAs of the analysed samples, using at least four dilution points and the efficiency of all primer sets was between 95 and 105%. Real-time PCR primer sequences were as follows: MICU1-fw, 5′-GTCGAACTCTCGGACCATGT-3′; MICU1-rv, 5′-CAAAGTCCCAGGCAGTTTCT-3′. These primers amplify a fragment of 199 base pairs. MCU-fw, 5′-AAAGGAGCCAAAAAGTCACG-3′; MCU-rv, 5′-AACGGCGTGAGTTACAAACA-3′. These primers amplify a fragment of 200 bp.

For the expression analysis of MCU silencing, total RNA was purified from HeLa cells transfected with scrambled, siRNA-MCU#1 and siRNA-MCU#2 for 48 h following the standard TRIzol protocol. The RNA was quantified, controlled for its quality and retrotranscribed as described earlier. Complementary DNA was analysed by real-time PCR using the SYBR Green chemistry (Bio-Rad). All data were normalized to *GAPDH* expression. The oligonucleotide primers specific for MCU are the same as above. The oligonucleotide primers specific for GAPDH are the following: GADPH-fw, 5′-CACCATCTTCCAGGAGCGAG-3′; GADPH-rv, 5′-CCTTCTCCATGGTGGTGAAGAC-3′. These primers amplify a fragment of 101 bp.

Constructs and siRNA. Mouse MCU (NM_001033259) was amplified from mouse skeletal muscle cDNA by PCR using the following primers.

For cloning into pEGFP-N1: fw, 5′-GAATTCGCCACCATGGCGGCCGCCGCAGGTAG-3′; rv, 5′-GGATCCACTTCCTTTTCTCCGATCTGTCG-3′. The PCR fragment was cloned into EcoRI and BamHI sites in pEGFP-N1 (Clontech).

For cloning into pcDNA3.1: fw, 5′-GGTACCGCCACCATGGCGGCCGCCGCAGGTAG-3′; rv, 5′-GAATTCTCATTCCTTTTCTCCGATCTGTC-3′. The PCR fragment was cloned into KpnI and EcoRI sites in pcDNA3.1 (Invitrogen).

For the cloning of MCU–Flag into pcDNA3.1: fw, 5′-GGTACCGCCACCATGGCGGCCGCCGCAGGTAG-3′; rv, 5′-GGAATTCTCACTTATCGTCGTCATCCTTGTAATCTTCCTTTTCTCCGATCTGTC-3′. The PCR fragment was cloned into KpnI and EcoRI sites in pcDNA3.1 (Invitrogen).

For the cloning of MCU in pET-28A(+): fw, 5′-AGGATCCATGGCGGCCGCCGCAGGTAG-3′; rv, 5′-ACTCGAGTCATTCCTTTTCTCCGATCT-3′. The PCR fragment was cloned into BamHI and XhoI sites in pET-28A(+) (Novagen).

For the cloning of MCU deleted of the mitochondrial targeting sequence (amino acids 1–54) ($MCU^{\Delta MTS}$) in pET-28A(+): fw, 5′-CATATGGCTTCCTGGCAGAGCGTGGG-3′; rv, 5′-CTCGAGTCATTCCTTTTCTCCGATCT-3′. The PCR fragment was cloned into NdeI and XhoI sites in pET-28A(+) (Novagen).

For the cloning of MCU in pIVEX 1.3 WG: fw, 5′-ACATATGGCGGCCGCCGCAGGTAGATC-3′; rv, 5′-TCTCGAGTTCCTTTTCTCCGATCTGTC-3′. The PCR fragment was cloned into NdeI and XhoI sites in pIVEX 1.3 WG (Roche).

The generation of the pcDNA3.1-$MCU^{D260Q,E263Q}$-Flag and pEGFP-N1-$MCU^{D260Q,E263Q}$ mutant was performed by mutagenesis PCR using the wild type pcDNA3.1-MCU-Flag and pEGFP-N1-MCU vectors as template and the mutagenesis primer: 5′-CTGGTGGGAGTACTCGTGGCAAATCATGCAACCCGTCACCTACTTCATCAC-3′.

Mouse MICU1 (NM_144822) was amplified from mouse skeletal muscle cDNA by PCR using the following primers:

For the cloning of MICU1-HA in pcDNA3.1: fw, 5′-CGGATCCGCCACCATGTTTCGTCTTAACACCCT-3′; rv, 3′-GCTCGAGTCACAGGGAAGCGTAGTCAGGCACATCGTAGGGGTATTTGGGCAGAGCAAAGTCCC-5′. The PCR fragment was cloned into BamHI and XhoI sites in pcDNA3.1 (Invitrogen).

For the cloning of MICU1 in pEGFP-N1: fw, 5′-CCTCGAGATGTTTCGTCTTAACACCCT-3′; rv, 5′-CGGATCCCGTTTGGGCAGAGCAAAGTCCC-3′. The PCR fragment was cloned into XhoI and BamHI sites in pEGFP-N1 (Clontech).

To silence MCU specific siRNA were designed: siRNA-MCU#1: nucleotides 899–917 of the corresponding mRNA (5′-GCCAGAGACAGACAAUACUtt-3′ and 3′-ttCGGUCUCUGUCUGUUAUGA-5′. siRNA-MCU#2: nucleotides 360–378 of the corresponding mRNA (5′-GGGAAUUGACAGAGUUGCUtt-3′and 3′-ttCCCUUAACUGUCUCAACGA-5′). The non-targeting siRNA (scrambled) is the following: 5′-GCCUAAGAACGACAAAUCAtt-3′ and 3′-ttCGGAUUCUUGCUGUUUAGU-5′.

Cell culture and transfection. In all the experiments HeLa cells were used. Cells were grown in Dulbecco's modified Eagle's medium (DMEM) (Euroclone), supplemented with 10% fetal bovine serum (FBS) (Euroclone) and transfected with a standard calcium-phosphate procedure. For aequorin measurements, the cells were seeded 24 h before transfection onto 13 mm glass coverslips and allowed to grow to 50% confluence before transfection. For morphologic analyses cells were seeded 24 h before transfection onto 24-mm glass coverslips and allowed to grow to 50% confluence before transfection, unless otherwise specified.

Aequorin measurements. HeLa cells grown on 13-mm round glass coverslips at 50% confluence were transfected with the cytosolic (cytAEQ) or the low-affinity mitochondrial (mtAEQmut, referred in the text as mtAEQ) probe (as previously described[25]) together with the indicated siRNA or plasmid. pcDNA3.1 was used as control unless otherwise indicated. The coverslip with the cells was incubated with 5 μM coelenterazine for 1–2 h in KRB (Krebs–Ringer modified buffer: 125 mM NaCl, 5 mM KCl, 1 mM Na_3PO_4, 1 mM $MgSO_4$, 5.5 mM glucose, 20 mM HEPES, pH 7.4, 37 °C) supplemented with 1 mM $CaCl_2$, and then transferred to the perfusion chamber. All aequorin measurements were carried out in KRB. Agonists and other drugs were added to the same medium, as specified in the text. The experiments were terminated by lysing the cells with 100 μM digitonin in a hypotonic Ca^{2+}-rich solution (10 mM $CaCl_2$ in H_2O), thus discharging the remaining aequorin pool. The light signal was collected and calibrated into $[Ca^{2+}]$ values by an algorithm based on the Ca^{2+} response curve of aequorin at physiological conditions of pH, $[Mg^{2+}]$ and ionic strength, as previously described[25]. Representative traces are shown in the figures whereas the full data set is included in Supplementary Table 2. In the experiments with permeabilized cells, a buffer mimicking the cytosolic ionic composition, (intracellular buffer) was used: 130 mM KCl, 10 mM NaCl, 2 mM K_2HPO_4, 5 mM succinic acid, 5 mM malic acid, 1 mM $MgCl_2$, 20 mM HEPES, 1 mM pyruvate, 0.5 mM ATP and 0.1 mM ADP (pH 7 at 37 °C). Intracellular buffer was supplemented with either 100 μM EGTA (intracellular buffer/EGTA) or a 2 mM EGTA and 2 mM HEEDTA-buffered $[Ca^{2+}]$ of 2 or 3 μM (intracellular buffer/Ca^{2+}), calculated with the Chelator software[28]. HeLa cells were permeabilized by a 1-min perfusion with 50 μM digitonin (added to intracellular buffer/EGTA) during luminescence measurements. Mitochondrial Ca^{2+} uptake speed was calculated as the first derivative by using the SLOPE Excel function (Microsoft) and smoothed for three time points. The higher value reached during Ca^{2+} addition represents the maximal Ca^{2+} uptake speed. $[Ca^{2+}]_{mt}$ following capacitative Ca^{2+} influx was measured by perfusing HeLa cells with the SERCA blocker cyclopiazonic acid (CPA, 20 μM) in a KRB solution containing no Ca^{2+} and 100 μM EGTA. In this protocol, mitochondrial Ca^{2+} uptake were evoked by adding 2 mM $CaCl_2$ to the medium. All of the results are expressed as means ± s.e.m., and Student's t-test was used for the statistics. All the materials were from Sigma Aldrich unless specified.

Mitochondrial and endoplasmic reticulum morphology analysis. Images for investigating mitochondrial morphology and endoplasmic reticulum/mitochondrial contact sites were taken on a Leica TCS-SP5-II equipped with a PlanApo 100×/1.4 numerical aperture objective. For all images, pinhole was set to 1 Airy unit, pixel size was 75 nm and a Z-stack was acquired for the whole depth of the cell by sampling at 130 nm in the Z plane. An argon laser line (488 nm) was used to excite GFP or AlexaFluor488 and the signal was collected in the 492–537 nm range, whereas RFP (and MitoTracker Red and AlexaFluor546) fluorescence was excited by the 543 nm HeNe laser and its emission was collected in the 555–700 nm range. For each image, PMT gain was slightly adjusted in order to maximize signal and avoid saturation. Images were then all analysed with the Fiji image processing package based on ImageJ. Mitochondrial morphology was calculated with the 3D Object Counter plugin, and colocalization was evaluated with the JaCoP plugin[29]. The colocalization index is represented by Pearson's coefficient calculated following Costes randomization (100 cycles) and automatic threshold calculation[30].

Immunofluorescence. HeLa cells were grown on 24-mm coverslips and transfected with MCU–Flag encoding plasmid when 50% confluent. After 24 h, cells were washed with PBS, fixed in 4% formaldehyde for 10 min and quenched with 50 mM NH_4Cl in PBS. Cells were permeabilized for 10 min with 0.1% Triton X-100 in PBS and blocked in PBS containing 2% BSA and 0.05% Triton X-100

for 1 h. Cells were then incubated with primary antibodies (anti-HSP60 and anti-Flag) for 3 h at room temperature and washed three times with 0.1% Triton X-100 in PBS. The appropriate isotype-matched, AlexaFluor-conjugated secondary antibodies (Invitrogen) were used and coverslips were mounted with ProLong Gold Antifade reagent (Invitrogen). Images were taken on a Leica SP5-II as detailed earlier.

Fractionation and western blotting. HeLa cells (10^8) were homogenized with a Dounce homogenizer (100 strokes) and centrifuged at 600*g* to remove entire cells. The supernatant was then centrifuged at 8,000*g* to pellet the crude mitochondrial fraction. Mitoplasts were obtained by osmotic swelling by incubating the mitochondrial fraction in 20 mM HEPES for 20 min. Proteins were quantified using the BCA Protein Assay Kit (Pierce) following the manufacturer instructions. Proteins (10 μg) were separated by SDS–PAGE, transferred onto nitrocellulose membranes (GE Healthcare) and probed using the following antibodies: anti-VDAC1(Abnova), anti-HSP60 (Santa Cruz) and anti-GFP (Abcam). Isotype-matched, horseradish-peroxidase-conjugated secondary antibodies (Bio-Rad) were used, followed by detection by chemiluminescence (GE Healthcare).

To test the siRNAs efficacy, HeLa cells were grown on 10-cm Petri dishes and transfected when 30% confluent. MCU–Flag encoding plasmid (8 μg) was co-transfected with scrambled, siRNA-MCU#1 or siRNA-MCU#2. After 72 h cells were washed, harvested and lysed in RIPA buffer (150 mM NaCl, 25 mM TRIS, 1% Triton-X100, 0.5% Na-deoxycholate and 0.1% SDS, pH 8) added with proteases and phosphatases inhibitor cocktails (Roche). Proteins were quantified by the bicinchoninic acid assay (BCA) method and 25 μg of each sample were loaded on a Novex NuPage Bis-Tris 4–12% precast gel (Invitrogen), transferred onto nitrocellulose membranes and probed with anti-β-tubulin (Sigma) and anti-Flag (Sigma) antibodies. Isotype-matched, horseradish-peroxidase-conjugated secondary antibodies (Bio-Rad) were used, followed by detection by chemiluminescence (GE Healthcare).

Measurements of mitochondrial ΔΨ. Mitochondrial ΔΨ was measured by loading cells with 20 nM tetramethyl rhodamine methyl ester (TMRM, Invitrogen) for 30 min at 37 °C. Images were taken on a inverted microscope (Zeiss Axiovert 100) equipped with a PlanFluar 40×/1.3 numerical aperture objective, a Photometrics Coolsnap ES and a LED-based illumination system (Cairn OptoLed II). TMRM excitation was performed at 560 nm and emission was collected through a 590–650 nm band-pass filter. Images were taken every 10 s with a fixed 200 ms exposure time. FCCP (carbonyl cyanide p-trifluoromethoxyphenylhydrazone, 10 μM), an uncoupler of oxidative phosphorylation, was added after 12 acquisitions to completely collapse the electrical gradient established by the respiratory chain (ΔΨ).

Trypan blue quenching experiment. After transfection with mtGFP, MCU–GFP or N33-D1cpV, cells were analysed on spinning disk imaging system composed of an inverted microscope (Zeiss Axiovert 200) equipped with a PlanApo 63×/1.4 numerical aperture objective, a BD-CARVII confocal head, a Photometrics Cascade 512B camera, a piezoelectric *Z* motor (Phisik instruments) and a 300 W Xenon bulb (Sutter Instruments). At each time point, a *Z*-stack was taken (*Z*-step: 500 nm) using standard EGFP filter-set (Semrock GFP-A-Basic-000) and the best focus plane was selected for subsequent analysis. After 1 min permeabilization in intracellular buffer containing 50 μM digitonin, cells were incubated in 1 ml of intracellular buffer, first treated with 4 units of proteinase K and then with 0.005% trypan blue. Best focus images of each time point were background-corrected and mitochondrial mean fluorescence intensity was measured with the MetaMorph software (Molecular devices).

Cell death experiment. Cell sensitivity to apoptotic stimuli was evaluated as previously described[12]. HeLa cells grown on 24-mm round glass coverslips at 30% confluence were transfected with MCU–GFP or GFP alone. The effect on cell fate was evaluated by applying an apoptotic challenge (40 μM C2-ceramide or 200 μM H_2O_2) and comparing the survival of transfected and non-transfected cells. In these experiments, the percentage of GFP-positive cells was calculated before and after applying an apoptotic stimulus (C2-ceramide or H_2O_2). In mock-transfected cells, although the total number of cells is reduced after cell death induction, the apparent transfection efficiency was maintained (that is, transfected and non-transfected cells have the same sensitivity to the apoptotic stimulus and thus die to the same extent). However, when cells are transfected with a construct influencing their sensitivity to apoptosis, this will be reflected by a change in the fraction of fluorescent cells, that is, in the 'apparent' transfection efficiency. Thus, protection from apoptosis results into an apparent increase of transfection, whereas a decrease reflects a higher sensitivity to apoptosis. Data are reported as the mean percentage change in the apparent transfection efficiency after apoptotic challenge compared to vehicle-treated cells. Cells were extensively washed with PBS, stained with 4′,6-diamidino-2-phenylindole (DAPI) and two images per field (blue and green fluorescence) were taken at 20× magnification (mean transfection efficiencies were roughly 30% for both GFP and MCU–GFP). At least 10 fields per coverslip were randomly imaged and counted. Data presented are the sum of at least two different coverslip per experimental condition carried out in three different independent experiments.

Immunogold electron microscopy. HeLa cells were transfected with control (pcDNA3.1) or MCU–Flag plasmids. Cells were fixed in 4% formaldehyde and 0.1% glutaraldehyde in 0.1 M cacodylate buffer 24 h after transfection. Dehydration was carried out by subsequent incubation with increasing ethanol concentrations (20, 40, 60, 80 and 100%). Cells were then infiltrated and embedded in LRW resin and 100-nm slices were obtained. For immunogold staining slices were first blocked in PBS containing 2% BSA and 0.05% Triton X-100 and then incubated for 1 h with anti-Flag (Sigma) antibody. After five washes with PBS, slices were incubated for 1 h with an isotype matched 10-nm gold-particles-conjugated secondary antibody (Sigma). After five washes with PBS and one wash with H_2O, slices were contrasted with uranyl acetate for 15 min and lead citrate for 6 min. Slices observation and imaging were carried out on a Tecnai G^2 TEM.

Protein expression and purification. *E. coli*: MCU and $MCU^{\Delta MTS}$ were cloned into the pET-28A(+) vector, as described above. Competent cells were transformed with the indicated constructs. Induction was performed at 20 °C ($D_{600} = 0.4$) with 0.35 mM isopropyl-β-D-thiogalactoside (IPTG) for 24 h. After sonication in buffer A (50 mM Na-phosphate, pH 7.4, 300 mM NaCl and protease inhibitor cocktail), the membranous fraction was collected by centrifugation (10 min at 12000*g*) and solubilized with *n*-decyl-β-D-maltopyranoside (2.5%) for 3 h at room temperature. The non-solubilized material was removed by centrifugation and the supernatant was loaded on a nickel chromatography column (HIS-Select Nickel affinity gel, Sigma). Column was washed with buffer A and the protein was eluted with imidazole gradient (50–200 mM). Fractions of 500 μl were collected and dialysed against buffer A without NaCl. A concentration of 0.025% of detergent was maintained throughout the purification.

In vitro: MCU was cloned into pIVEX 1.3 WG, as described above. *In vitro* expression was performed by using a RTS100 Wheat Germ CECF Kit (Roche). After expression, the reaction mix was solubilized with 2% Triton X-100 for 90 min at 30 °C under shaking.

Gel electrophoresis: SDS–PAGE was performed using 6 M urea and standard protocols. Each lane was loaded with 30 μl of eluted fractions and 1 μl of the reaction mix.

Electrophysiology. Electrophysiology experiments were carried out as previously described[31,32]. A Warner Instruments (Hamden) electrophysiological planar bilayer apparatus was used. Bilayers of approximately 150–200 pF capacity were prepared using azolectin in decane containing 1% chloroform (Sigma) across a 250 μM hole in a polystyrene cuvette. Azolectin was partially purified by precipitation with cold acetone from a chloroform solution. The inside of the cuvette constituted the *trans* compartment. The standard experimental medium was 100 mM $CaCl_2$ (or Ca-gluconate), 10 mM HEPES/pH 7.2. The lipid membrane was built under symmetric ionic conditions and both chambers contained 3 ml of solution. The contents of both chambers were stirred by magnetic bars when desired. Connections to the electrodes were provided by agar bridges. Purified proteins were added to the *cis* side. Control experiments with empty membrane or with detergents used for the purification showed no activity. All voltages reported are those of the *cis* chamber, zero being assigned by convention to the *trans* (grounded) side. Currents are considered as positive when carried by cations flowing from the *cis* to the *trans* compartment. A BC-525C unit and headstage were used to control parameters and amplify signals. Output was recorded with a 10 kHz bandwidth on videotape using a Medical Systems PCM-2 interface. Data were acquired at 2 kHz, filtered at 500 Hz and analysed offline using the pClamp program set (Axon Instruments). Conductance was determined by averaging the measured amplitudes of single channel events ($n \geq 50$) at various applied voltages.

Statistical analysis of data. Statistical data are presented as mean ± s.e.m., unless otherwise specified. Significance was calculated by Student's *t*-test, and correlation analysis was performed with the SigmaPlot 11.0 software (Systat Software Inc.).

27. Krogh, A., Larsson, B., von Heijne, G. & Sonnhammer, E. L. Predicting transmembrane protein topology with a hidden Markov model: application to complete genomes. *J. Mol. Biol.* **305,** 567–580 (2001).
28. Schoenmakers, T. J. M., Visser, G. J., Flik, G. & Theuvenet, A. P. R. CHELATOR: an improved method for computing metal ion concentrations in physiological solutions. *Biocomputing* **12,** 870–879 (1992).
29. Bolte, S. & Cordelieres, F. P. A guided tour into subcellular colocalization analysis in light microscopy. *J. Microsc.* **224,** 213–232 (2006).
30. Costes, S. V. *et al.* Automatic and quantitative measurement of protein-protein colocalization in live cells. *Biophys. J.* **86,** 3993–4003 (2004).
31. Szabò, I., Soddemann, M., Leanza, L., Zoratti, M. & Gulbins, E. Single-point mutations of a lysine residue change function of Bax and Bcl-x_L expressed in Bax- and Bak-less mouse embryonic fibroblasts: novel insights into the molecular mechanisms of Bax-induced apoptosis. *Cell Death Differ.* **18,** 427–438 (2011).
32. Teardo, E. *et al.* Characterization of a plant glutamate receptor activity. *Cell. Physiol. Biochem.* **26,** 253–262 (2010).